sciendo Radiology and Oncology | Ljubljana | Slovenia | www.radioloncol.com RADIOLOGY AND ONCOLOGY

research article

Correlations between DTI-derived metrics and MRS metabolites in tumour regions of glioblastoma: a pilot study

Eduardo Flores-Alvarez[1], Edgar-Anselmo Rios-Piedra[2], Griselda-Adriana Cruz-Priego[3], Coral Durand-Muñoz[4], Sergio Moreno-Jimenez[5], Ernesto Roldan-Valadez[6,7]

[1] Department of Neurosurgery, General Hospital of Mexico, Secretariat of Health, Mexico City, Mexico
[2] Department of Radiology, Stanford University, CA, USA; Department of Electrical Engineering, Stanford University, CA, USA
[3] Postgraduate Unit, Faculty of Medicine, National Autonomous University of Mexico, Mexico City, Mexico
[4] Department of Internal Medicine, Medica Sur Clinic and Foundation, Mexico City, Mexico
[5] Radioneurosurgery Unit, The National Institute of Neurology and Neurosurgery, Mexico City, Mexico
[6] Department of Radiology, I.M. Sechenov First Moscow State Medical University (Sechenov University), Moscow, Russia
[7] Directorate of Research, General Hospital of Mexico, Secretariat of Health, Mexico City, Mexico

Radiol Oncol 2020; 54(4): 394-408.

Received 9 July 2020
Accepted 31 July 2020

Correspondence to: Ernesto Roldan-Valadez, M.D., M.Sc., D.Sc., Department of Radiology, I.M. Sechenov First Moscow State Medical University (Sechenov University), Trubetskaya str., 8, b. 2, 119992, Moscow, Russia. Email: ernest.roldan@usa.net

Disclosure: No potential conflicts of interest were disclosed.

Introduction. Specific correlations among diffusion tensor imaging (DTI)-derived metrics and magnetic resonance spectroscopy (MRS) metabolite ratios in brains with glioblastoma are still not completely understood.

Patients and methods. We made retrospective cohort study. MRS ratios (choline-to-N-acetyl aspartate [Cho/NAA], lipids and lactate to creatine [LL/Cr], and myo-inositol/creatine [mI/Cr]) were correlated with eleven DTI biomarkers: mean diffusivity (MD), fractional anisotropy (FA), pure isotropic diffusion (p), pure anisotropic diffusion (q), the total magnitude of the diffusion tensor (L), linear tensor (Cl), planar tensor (Cp), spherical tensor (Cs), relative anisotropy (RA), axial diffusivity (AD) and radial diffusivity (RD) at the same regions: enhanced rim, peritumoral oedema and normal-appearing white matter. Correlational analyses of 546 MRS and DTI measurements used Spearman coefficient.

Results. At the enhancing rim we found four significant correlations: FA ⇔ LL/Cr, Rs = -.364, p = .034; Cp ⇔ LL/Cr, Rs = .362, p = .035; q ⇔ LL/Cr, Rs = -.349, p = .035; RA ⇔ LL/Cr, Rs = -.357, p = .038. Another ten pairs of significant correlations were found in the peritumoral edema: AD ⇔ LL/Cr, AD ⇔ mI/Cr, MD ⇔ LL/Cr, MD ⇔ mI/Cr, p ⇔ LL/Cr, p ⇔ mI/Cr, RD ⇔ mI/Cr, RD ⇔ mI/Cr, L ⇔ LL/Cr, L ⇔ mI/Cr.

Conclusions. DTI and MRS biomarkers answer different questions; peritumoral oedema represents the biggest challenge with at least ten significant correlations between DTI and MRS that need additional studies. The fact that DTI and MRS measures are not specific of one histologic type of tumour broadens their application to a wider variety of intracranial pathologies.

Key words: brain neoplasms; diffusion tensor imaging; magnetic resonance spectroscopy; statistics as topic; software tools

Introduction

Since the last decade, a particular interest prevails for the identification of clinical prognostic markers for glioblastoma.[1] During this time, medical imaging research has focused its attention in the conventional magnetic resonance imaging (MRI) diagnosis of gliomas, identifying regional tumour infiltration and oedema boundaries in those qualitative patterns observed in the T_2-weighted imaging (T_2-w), fluid-attenuated inversion recovery (FLAIR), pre-contrast T_1-w weighted imaging

(T_1-w), and post-contrast T_1-w.[2] Other MRI-based quantitative morphological features that have been reported include the contrast-enhancing (CE) rim width and surface regularity[3], residual tumour volume (RTV) and extent of resection (EOR).[4] A recent meta-analysis highlighted the limitations of the current conventional MRI-based Response Assessment in Neuro-Oncology (RANO) criteria for treatment evaluation in glioblastoma.[5]

Some volumetric features of the oedema region might have a role as predictors of progression-free survival (PFS) in patients with glioblastoma.[6]

Diffusion tensor imaging (DTI) and magnetic resonance spectroscopy (MRS) biomarkers are currently reported in glioblastoma research as a consequence of their higher diagnostic accuracy than conventional MRI for the detection of tumour progression.[7,8] A recent meta-analysis found the sensitivity and specificity of MRS were 91% and 95%, respectively.[9] MRS found that the choline-to-N-acetyl aspartate (Cho/Naa) ratio is the most substantial survival predictor in glioblastoma with a log-hazard function of 2.672 (each unit of increase in the Cho/Naa ratio represents a 267% increase in the risk of death in glioblastoma).[10] The usefulness of DTI-derived biomarkers has been proved in the differentiation of glioblastoma from brain abscesses and metastatic brain tumours[11] and between glioblastoma and healthy brains.[12] Up to 11 DTI-derived biomarkers have calculated in brain MRI, each one with different diagnostic performance depending on the selected tumour region.[13]

However, despite the above technological advances in glioblastoma imaging, there is a low correlation between the conventional MR images and the gross pathologic margin of the tumour with the actual margins of the areas of neoplastic infiltration.[14] Most of the advanced MRI techniques have been reported as separated diagnostic methods without a correlational assessment.[5] For example, some studies have been published about the whole brain MRS correlations with Sox2-positive cell density[8], but no with other advanced MRI techniques. We found only one article in the literature that studied the correlations between DTI and MRS in schizophrenic patients and healthy controls.[15] Although it is known that MRS and DTI use different mechanisms to visualizer abnormal pathologies, they can provide complementary imaging data on white matter changes in brain.[15]

The assessment of MRS and DTI biomarkers in glioblastoma is one of the leading research lines for our group. To the best of our knowledge, no previous studies have evinced a correlation among these variables; we aimed to analyse the correlations between the three most commonly reported MRS metabolites ratios and the eleven-known DTI-derived metrics in glioblastoma. Our null hypothesis considered no correlations between MRS metabolite ratios and DTI metrics; our alternative hypothesis expects that at least one pair of significant correlations were found at each tumour region in glioblastoma.

Patients and methods

Patients

Retrospective cohort of patients with at first (suspected) diagnosis and later pathology confirmation of glioblastoma according to the WHO; inclusion criteria considered examinations between January 2010 and December 2014. Exclusion criteria applied to corticosteroid or antibiotic treatment, lesions with areas related to calcification and haemorrhage and previous brain surgery. MR examinations with other structural abnormalities were excluded. The local Institutional Review Board approved the study and the study was performed in accordance with the ethical standards laid down in the 1964 Declaration of Helsinki and its later amendments.

Brain image acquisition

MR was performed by using a 3T unit (Signa HDxt, GE Healthcare, Waukesha, WI, USA) with a high-resolution eight-channel head coil (Invivo, Gainesville, FL, USA). MR sequences included conventional axial T_2-w, axial Fluid-Attenuated Inversion Recovery (Flair), and pre-contrast axial T_1-w. Post-contrast axial T_1-w used 0.1 mmol/kg of body weight of gadopentetate dimeglumine (Magnevist; Schering, Berlin, Germany). Pre-contrast axial Spoiled Gradient Echo (SPGR) that exploited the T1 shortening effects of methemoglobin allowed direct visualization of lesions with haemorrhage. Diffusion-weighted imaging (DWI) was performed using a single-shot SE EPI sequence with b-values of 1000 s/mm^2 and an image without diffusion weighting with b-value of 0 s/mm^2.

DTI was performed using a single-shot SE EPI sequence. Diffusion gradients were applied in 25 directions with b-values of 1000 s/mm^2 and an image without diffusion weighting with b-value of 0 s/mm^2. DTI sequences were acquired in the axial plane with 44 contiguous sections, 2.4 mm section thickness, no intersection gap, TR/TE of 17,000/80 ms, with parallel imaging to reduce off-resonance

artefacts (PI factor was 2); 25 x 25 cm FOV, and 128 x 128 matrix size.

Selected tumour regions

A board-certified radiologist (ERV) blinded to the clinical history of each patient, manually traced the boundaries of the tumour regions. For all parameters derived from MRS and DTI, measurements were acquired in three areas: normal-appearing white matter (NAWM), drawn in the patient's contralateral hemisphere; viable tumour region (area of the enhanced rim at T1-w post-contrast); and peritumoral oedema (arbitrarily chosen as an adjacent immediate zone with a 10-mm-wide band).

Metabolites measurements using MRS

Multi-voxel spectroscopic imaging (MV-MRS) was performed using a point-resolved spectroscopic sequence technique (PRESS). The volume of interest (VOI) size was individually adjusted positioning the voxel over the lesion and trying to minimise partial-volume effects resulting from other neighbouring tissues including bones and cerebral spinal fluid (CSF) of the ventricles. Proton spectra were recorded in the axial plane with T1-w post-contrast images via TR; 1500 ms, TE; 26 and 144 ms, FOV; 24 × 24 cm, 1–1.5 cm section thickness, 256 × 256 matrix and 24 × 24 phase encoding. Knowing that cerebral metabolites have different inherent T1 and T2 relaxation times, a TE of 24 ms allowed us to quantify metabolites that are identified only at short TE (Lipids and Myo-inositol). The intermediate TE of 144 ms let us identified the Cho and Lactate peaks, which are the primary metabolites altered in neoplasms. Because fewer metabolites were observed with longer TE values, the spectrum obtained is easier to interpret (we could quickly identify the rest of selected metabolites (NAA and Cr). Additionally, a TE of 144 ms identified the Lactate peak invert below baseline.[16]

The MRS data were transferred to a clinical workstation, with FDA-cleared software (GE Advantage). A short echo time allowed the acquisition of four brain spectra with metabolite signal peaks centred within a range of 0–4.35 ppm as follows: methyl protons of N-acetylaspartate (NAA) at 2.0 ppm, N-trimethyl protons of choline-containing metabolites at 3.2 ppm (Cho), creatine (Cr) at 3–3.1 ppm, a compound peak containing lipids and lactate (LL) at 0.8–1.4 ppm, and a compound peak of the protons of myo-inositol (mI) at 3.56 and 4.06 ppm.[16] Automatic shimming of the linear x, y, z channels was used to optimise field homogeneity, water resonance and water suppression pulses were optimised. Relative quantification of metabolites was performed after Gaussian curve fitting using standard spectroscopic analysis software FuncTool 9.4.04b, (GE Healthcare, Milwaukee, WI, USA). Three metabolite ratios were calculated: Cho/NAA, lipids and lactate to creatine (LL/Cr), and and myo-inositol/creatine (mI/Cr). Figure 1 A–F show examples of the MRS measurements at the enhancing rim and peritumoral oedema.

DTI-derived metrics

We used the FA maps, and T_1-post gadolinium orientation maps to draw three regions of interest (ROI) from each selected region (NAWM, enhancing rim and peritumoral oedema). For each ROI, we obtained the major (λ1), intermediate (λ2), and minor (λ3) eigenvalues at the selected regions using a GE Advantage Workstation with the software FuncTool 9.4.04b (GE Medical Systems, Milwaukee, WI, USA). The three eigenvalues were applied to the eleven formulas previously published for the calculation of DTI-derived metrics: mean diffusivity (MD), fractional anisotropy (FA), pure isotropic diffusion (p), pure anisotropic diffusion (q), the total magnitude of the diffusion tensor (L), linear tensor (Cl), planar tensor (Cp), spherical tensor (Cs), relative anisotropy (RA), axial diffusivity (AD) and radial diffusivity (RD)[13]; Figure 1 G–I presents an example of FA map used to locate the ROI at the selected regions: enhancing rim, peritumoral oedema, and NAWM.

Statistical analysis

Sample size

We used the sample-size formula published by Browner *et al.* for determining whether a correlation coefficient differs from zero.[17]

$N = [(Z\alpha + Z\beta) \div C]^2 + 3$, for this formula:

N = Total number of measurements required

Zα = the standard normal deviate for α (If the alternative hypothesis is two-sided, Zα = 1.96 when α = 0.05)

Zβ = the standard normal deviate for β (Zβ = 0.84 when β = 0.20)

$C = 0.5 \times \ln [(1 + r)/(1 - r)]$

r = expected correlation coefficient

Considering that Tang *et al*. reported a correlation coefficient between DTI and MRS biomarkers up to 33.2% in schizophrenic patients[15], our alternative hypothesis was that correlation coefficients

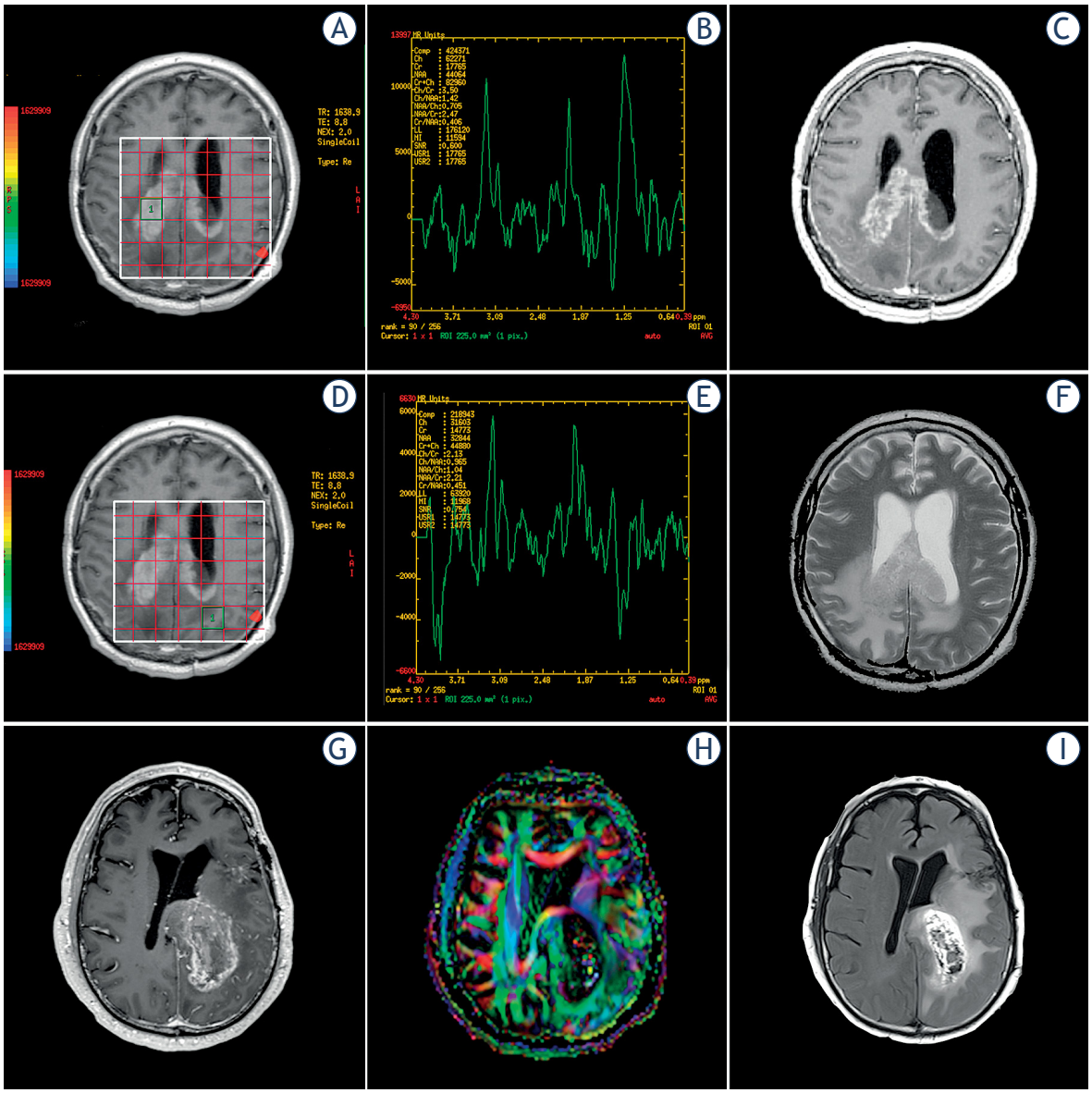

FIGURE 1. (A-F) magnetic resonance spectroscopy (MRS) measurements at the enhancing rim and peritumoral edema. **(G-I)** example of a FA map used to locate the ROI at the selected regions: enhancing rim, peritumoral oedema, and normal-appearing white matter (NAWM).

between DTI and MRS biomarkers would be above 50%. With this expected correlation coefficient, a two-sided alternative hypothesis, $\alpha = 0.05$, $\beta = 0.20$, and statistical power = 80%; N = 29. We had 33 different measurements per each DTI biomarkers.

Correlation analyses

Bivariate correlations were performed using the Spearman correlation coefficient (R_s)[18] to describe the degree of the linear relationship between three metabolites ratios (Cho/Naa, LL/Cr, and mI/Cr) and the eleven DTI-derived biomarkers (MD, FA, p, q, L, Cl, Cp, Cs, RA, AD and RD). We chose the Rs because it is a non-parametric test that can be used with variables that have a non-normal distribution.[19] Each correlation coefficient was interpreted as *Very strong* (at least of 0.8), *Moderately strong* (0.6 up to 0.8), *Fair* (0.3 up to 0.6) and *Poor* (less than 0.3). Squaring R-values represented the *coefficient of determination*, the proportion of variance that each two compared variables had in common.[18] We additionally tested the statistical significance of the difference between R coefficients between groups

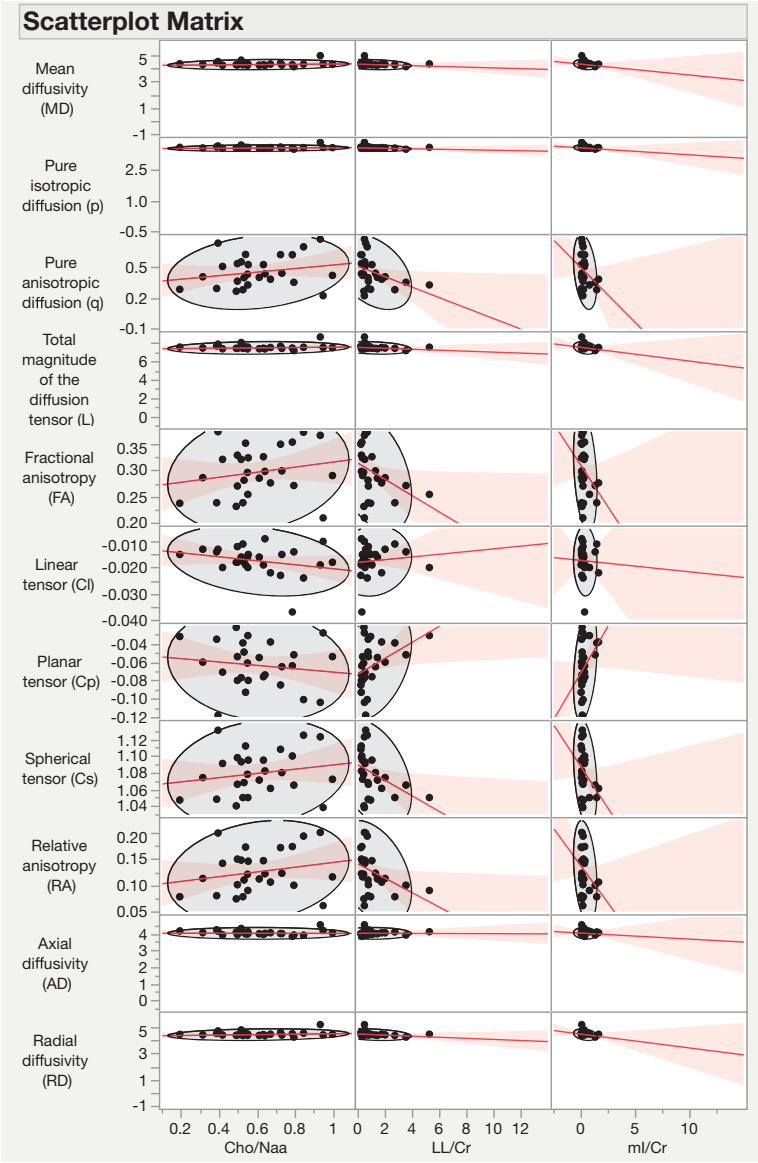

FIGURE 2. Scatter plots showing the correlation between magnetic resonance spectroscopy (MRS) metabolites and diffusion tensor imaging (DTI) metric at the normal-appearing white matter (NAWM).

by converting each pair of R values into standard z scores, then using the formula proposed by Pallant and colleagues[20]:

$$Z_{obs} = \frac{Z_1 - Z_2}{\sqrt{\frac{1}{N_1 - 3} + \frac{1}{N_2 - 3}}}$$

Observed Z value (Z_{obs}) ≤ -1.96 or ≥ 1.96 were considered statistically significantly different.

Software

All analyses were carried out using the IBM® SPSS® Statistics software (version 26.0.0.1 IBM Corporation; Armonk, NY, USA) and JMP® Pro software (version 14.3, SAS Institute Inc., Cary, NC, USA). Statistical significance was indicated by $p < 0.05$ (two-tailed).

Results

DTI and MRS measurements

For each patient, we recorded MRS and DTI measurements at three selected regions: NAWM, enhancing rim and oedema. The three MRS measures for each metabolite ratio (Cho/Naa, LL/Cr, and mI/Cr) were recorded at all tumour region, adding 9 MRS measurements per patient. Similarly, 11 DTI-derived metrics (MD, FA, p, q, L, Cl, Cp, Cs, RA, AD and RD) were calculated at each tumour region for each patient, with a total of 33 DTI measurements. Then, for each patient, we got 42 measurements (9 from MRS and 33 from DTI), this amount multiplied by 13 patients added 546 measurements that integrated 33 MRS-DTI parameter pairs per region. A total of 99 bivariate pairs were obtained in our correlation analyses.

DTI⇔MRS correlation at the NAWM

We found five pairs of bivariate correlations showing statistical significance all of them with the same metabolite LL/Cr. Only one correlation was positive, Cp ⇔ LL/Cr, R_s = .468, p = .014. The other four depicted negative Rs coefficients: FA ⇔ LL/Cr, R_s = -.475, p = .012; q ⇔ LL/Cr, R_s = -.495, p = .009; RA ⇔ LL/Cr, R_s = -.490, p = .010; Cs ⇔ LL/Cr, R_s = -.488, p = .010. Table 1 shows the correlations between DTI metrics and MRS metabolites at the NAWM region. Figure 2 depicts a scatterplot matrix of the DTI and MRS correlations at the NAWM region.

DTI⇔MRS correlation at the gadolinium-enhanced tumour region

Similar to the findings in the NAWM, we found only four significant correlations between only one MRS metabolite and 4 DTI-derived metrics: FA ⇔ LL/Cr, R_s = -.364, p = .034; Cp ⇔ LL/Cr, R_s = .362, p = .035; q ⇔ LL/Cr, R_s = -.349, p = .035; RA ⇔ LL/Cr, R_s = -.357, p = .038. Table 2 depicts the correlations between DTI metrics and MRS metabolites at the tumor region. Figure 3 show a scatterplot matrix of the DTI and MRS correlations at the enhancing rim region.

TABLE 1. Correlations between diffusion tensor imaging (DTI) metrics and magnetic resonance spectroscopy (MRS) metabolites for the normal-appearing white matter (NAWM) region

DTI-derived biomarker	MRS	Spearman ρ	p-value
Axial diffusivity (AD)	Cho/Naa	-0.2862	0.1479
	LL/Cr	0.1900	0.3426
	ml/Cr	-0.1777	0.3751
Fractional anisotropy (FA)	Cho/Naa	0.2300	0.2485
	LL/Cr	-0.4749	**0.0123***
	ml/Cr	-0.2110	0.2907
Linear tensor (Cl)	Cho/Naa	-0.2827	0.1530
	LL/Cr	0.2061	0.3024
	ml/Cr	-0.2147	0.2822
Mean diffusivity (MD)	Cho/Naa	-0.0961	0.6336
	LL/Cr	-0.1020	0.6126
	ml/Cr	-0.2683	0.1761
Planar tensor (Cp)	Cho/Naa	-0.1441	0.4732
	LL/Cr	0.4680	**0.0138***
	ml/Cr	0.3139	0.1108
Pure anisotropic diffusion (q)	Cho/Naa	0.2119	0.2886
	LL/Cr	-0.4950	**0.0087***
	ml/Cr	-0.2577	0.1944
Pure isotropic diffusion (p)	Cho/Naa	-0.0961	0.6336
	LL/Cr	-0.1020	0.6126
	ml/Cr	-0.2683	0.1761
Radial diffusivity (RD)	Cho/Naa	0.0440	0.8276
	LL/Cr	-0.2840	0.1511
	ml/Cr	-0.2228	0.2640
Relative anisotropy (RA)	Cho/Naa	0.2217	0.2665
	LL/Cr	-0.4898	**0.0095***
	ml/Cr	-0.2290	0.2506
Spherical tensor (Cs)	Cho/Naa	0.1930	0.3348
	LL/Cr	-0.4883	**0.0098***
	ml/Cr	-0.2547	0.1998
Total magnitude of the diffusion tensor (L)	Cho/Naa	-0.0680	0.7363
	LL/Cr	-0.1408	0.4836
	ml/Cr	-0.2781	0.1602

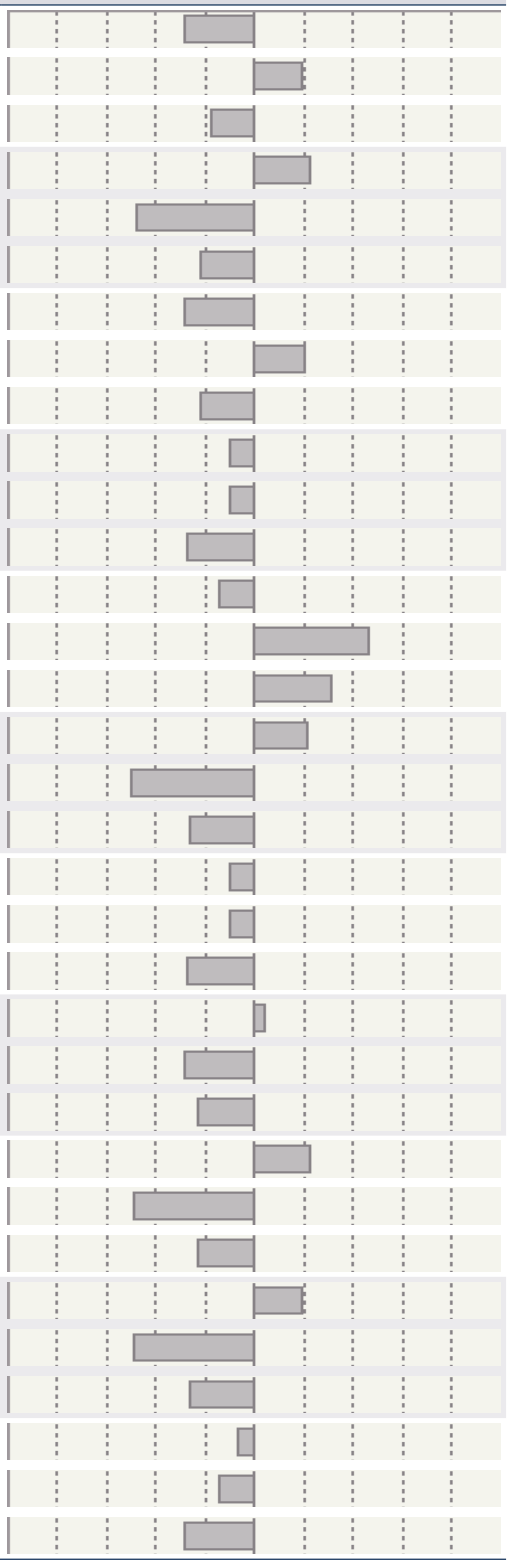

Cho/Naa = choline-to-N-acetyl aspartate; LL/Cr = lipids and lactate to creatine; ml/Cr = and myo-inositol/creatine [ml/Cr]

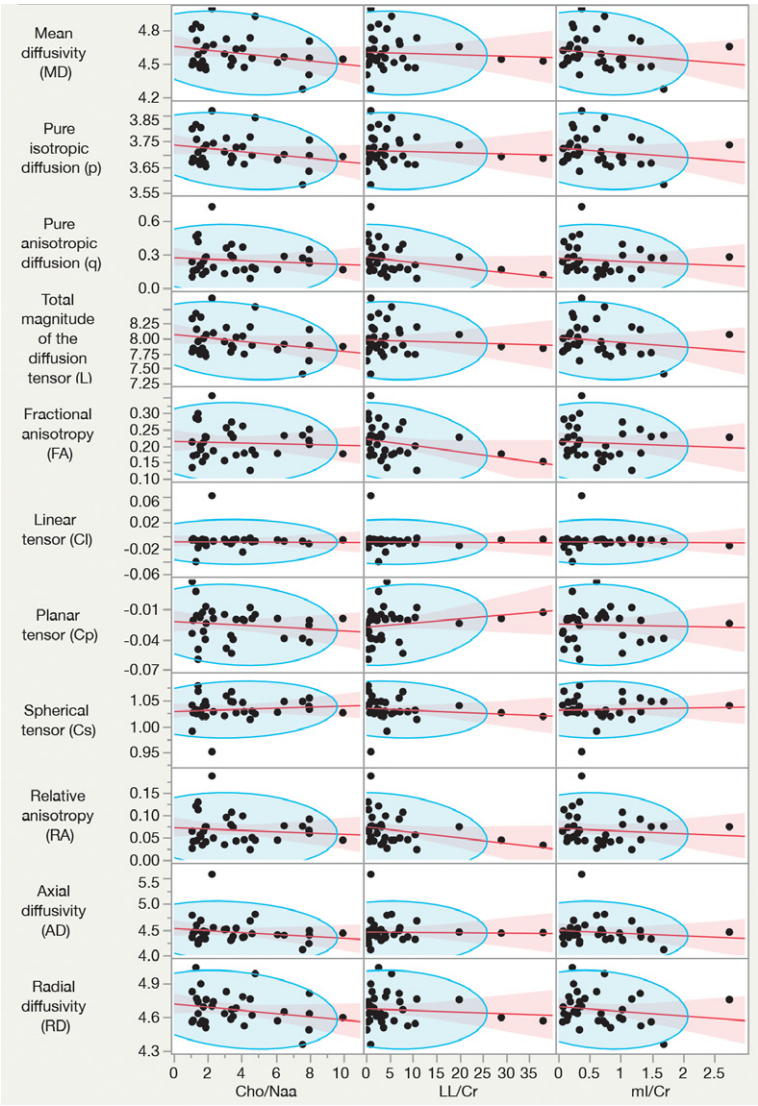

FIGURE 3. Scatter plots showing the correlation between magnetic resonance spectroscopy (MRS) metabolites and diffusion tensor imaging (DTI) metric at the enhancing rim.

DTI⇔MRS correlation at the oedema region

At the edema region we found that besides the LL/Cr metabolite, the concentrations of mI/Cr also depicted statistical significance with five DTI metrics different than the observed correlations in the tumor and NAWM regions. It meant we found ten significand correlations: AD ⇔ LL/Cr, R_s = .658, p < .001; AD ⇔ mI/Cr, R_s = .493, p = .006; MD ⇔ LL/Cr, R_s = .685, p < .001; MD ⇔ mI/Cr, R_s = .513, p = .004; p ⇔ LL/Cr, R_s = .685, p < .001; p ⇔ mI/Cr, R_s = .513, p = .004; RD ⇔ mI/Cr, R_s = .693, p < .001; RD ⇔ mI/Cr, R_s = .508, p = .004; L ⇔ LL/Cr, R_s = .685, p < .001; L ⇔ mI/Cr, R_s = .513, p = .004. Table 3 presents the correlations between DTI metrics and MRS metabolites at the edema region. Figure 4 show a scatterplot matrix of the DTI and MRS correlations at the peritumoral edema. Figure 5 depicts a diagram showing the significant correlations observed between DTI-MRS bivariate correlations at the NAWN, tumor and edema regions.

Statistical significance between identical DTI-MRS bivariate pairs in different regions

The assessment of the statistical significance of the difference between R coefficients found only four pairs of DTI-MRS correlations that were coincidentally significant at NAWM and tumor enhanced regions (Figure 4). We did not find statistical significances between their R coefficients: Cp ⇔ LL/Cr, Z = .54, p = .589; FA ⇔ LL/Cr, Z = .57, p = .568; q ⇔ LL/Cr, Z = .76, p = .447; RA ⇔ LL/Cr, Z = .69, p = .490.

Discussion

Between 1998 and 2009, quantitative biomarkers from MRS (NAA, Cho, LL, and mI) were accepted to be measured with sufficient sensitivity in the millimoles per litre range to be used in clinical diagnosis.[21] Recent studies have shown the importance of Cho/NAA and LL/Cr ratios in assembling significant survival models in glioblastoma.[10] The use of DTI allows *diffusion directionality* to be quantified as different DTI-derived metrics[21]; it yields ultrastructural information on cellular density and properties of the extracellular matrix.[22] In 2006, Pena *et al.* expressed that it was not completely understood the magnitudes and associations among DTI measurements observed in the evaluation of brain tumours.[23] Cortez-Conradis *et al.* in 2015, evaluated correlations among DTI-derived metrics in glioblastoma[24], but without exploring the associations with MRS metabolites in the same tumour regions.

In this study, we were able to probe the alternative hypothesis posed at the introduction and methods sections: bivariate correlations among DTI-metrics and MRS metabolite ratios are significant at selected tumour regions and above 50% of Rs value in glioblastoma (NAWM, enhancing rim and peritumoral oedema). To the best of our knowledge, there are no similar studies in the literature with whom compare our findings.

TABLE 2. Correlations between diffusion tensor imaging (DTI) metrics and magnetic resonance spectroscopy (MRS) metabolites for the tumour region

DTI-derived biomarker	MRS	Spearman ρ	p-value	-.8 -.6 -.4 -.2 0 .2 .4 .6 .8
Axial diffusivity (AD)	Cho/Naa	-0.0961	0.5886	
	LL/Cr	0.2044	0.2463	
	ml/Cr	-0.0824	0.6432	
Fractional anisotropy (FA)	Cho/Naa	0.0165	0.9262	
	LL/Cr	-0.3643	**0.0342***	
	ml/Cr	-0.1238	0.4855	
Linear tensor (Cl)	Cho/Naa	0.0017	0.9924	
	LL/Cr	0.0674	0.7048	
	ml/Cr	0.0395	0.8246	
Mean diffusivity (MD)	Cho/Naa	-0.1152	0.5167	
	LL/Cr	0.0790	0.6569	
	ml/Cr	-0.1713	0.3327	
Planar tensor (Cp)	Cho/Naa	-0.1699	0.3369	
	LL/Cr	0.3629	**0.0349***	
	ml/Cr	0.0604	0.7342	
Pure anisotropic diffusion (q)	Cho/Naa	0.0003	0.9986	
	LL/Cr	-0.3488	**0.0432***	
	ml/Cr	-0.1394	0.4317	
Pure isotropic diffusion (p)	Cho/Naa	-0.1152	0.5167	
	LL/Cr	0.0790	0.6569	
	ml/Cr	-0.1713	0.3327	
Radial diffusivity (RD)	Cho/Naa	-0.1478	0.4040	
	LL/Cr	0.0558	0.7539	
	ml/Cr	-0.1839	0.2978	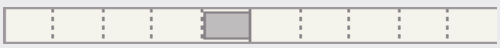
Relative anisotropy (RA)	Cho/Naa	0.0200	0.9105	
	LL/Cr	-0.3569	**0.0382***	
	ml/Cr	-0.1241	0.4843	
Spherical tensor (Cs)	Cho/Naa	0.0983	0.5804	
	LL/Cr	-0.3188	0.0661	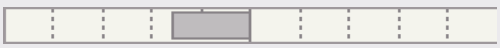
	ml/Cr	-0.0944	0.5953	
Total magnitude of the diffusion tensor (L)	Cho/Naa	-0.1232	0.4877	
	LL/Cr	0.0799	0.6532	
	ml/Cr	-0.1606	0.3643	

Cho/Naa = choline-to-N-acetyl aspartate; LL/Cr = lipids and lactate to creatine; ml/Cr = and myo-inositol/creatine

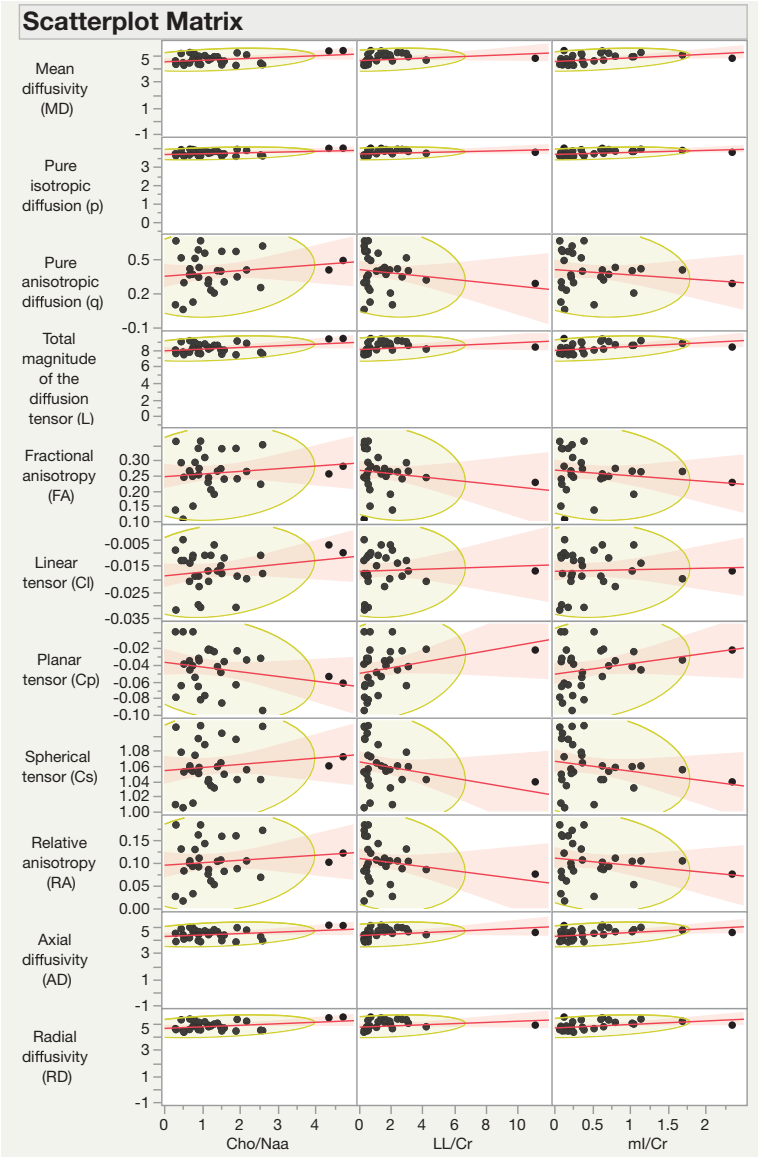

FIGURE 4. Scatter plots showing the correlation between magnetic resonance spectroscopy (MRS) metabolites and diffusion tensor imaging (DTI) metric at the peritumoral edema.

The clinical relevance of our findings is the statistical evidence that DTI and MRS depict significant associations in glioblastoma. MRS measurements represent a biochemical profile of brains with glioblastoma: decreased N-acetylaspartate (NAA) is a putative indicator of persistent axonal damage; increases of choline and myo-inositol correspond to glial proliferation, and elevated lactate has been associated with inflammation.[25] DTI metrics measure the amount of coherence of water diffusion, which putatively reflects the amount of myelination in axonal bundles or the coherence of fibre tracts.[15] Although DTI and MRS reflect different mechanisms of damage by glioblastoma, together they provide complementary imaging data on white matter integrity in brain. The supplementary information provided by DTI and MRS is what we consider the rationale of our study, both techniques should complement the information from conventional MRI in day-to-day practice. The clinical implications will allow researchers to combine DTI and MRS metrics to test several prediction models for tumour progression or the presence of tumour cells in peritumoral oedema and decrease the patient-to-patient prognostic variability. For example, you could combine the variables of two significant bivariate pairs with Rs > 65% in our study (for example AD ⇔ LL/Cr and RD ⇔ mI/Cr measured in peritumoral oedema) together with age, in a Cox's proportional-hazards regression model for prediction of survival. The results might be compared with previously published models.[10]

To simplify the discussion of our findings, we grouped them into four sections:

Lack of significant correlations between Cho/NAA and any of the 11 DTI biomarkers in the three selected regions

This was the first finding that caught our attention. To explain this fact, we should remember that Cho peak is the most complex, receiving contributions from a range of choline-containing compounds (acetylcholine, glycerophosphocholine, phosphocholine, free choline, phosphatidylcholine and choline-plasmalogen); its concentration is frequently taken as an empirical marker of the density and turnover of cell membranes.[26] Because increased Cho may be seen in diverse pathologies like infarction (from gliosis or ischemic damage to myelin) or inflammation (glial proliferation); it is considered to be nonspecific.[26] NAA is present in the soma of neurons, in dendrites and axons, its regional variability is likely related to differences in neural architecture, population and density. A simple linear relationship of NAA with the mass of neurons has been considered unlikely given that it also reflects reversible metabolic changes.[27] A high concentration of Cho has been observed in brain tumours and *in vitro* tumour proliferation markers with Cho/NAA ratio significantly more elevated in high-grade gliomas than in low-grade gliomas. However, threshold values are not well established.[28] glioblastoma exhibit high choline-containing compound levels, especially in the tumour regions, Cho/NAA quantifies those lipid components, and the DTI-derived metrics evaluates ultra-

TABLE 3. Correlations between diffusion tensor imaging (DTI) metrics and magnetic resonance spectroscopy (MRS) metabolites for the oedema region

DTI-derived biomarker	MRS	Spearman ρ	p-value	-.8 -.6 -.4 -.2 0 .2 .4 .6 .8
Axial diffusivity (AD)	Cho/Naa	0.0913	0.6315	
	LL/Cr	0.6575	**<.0001***	
	ml/Cr	0.4926	0.0057*	
Fractional anisotropy (FA)	Cho/Naa	0.0939	0.6217	
	LL/Cr	-0.2817	0.1316	
	ml/Cr	-0.1444	0.4465	
Linear tensor (Cl)	Cho/Naa	0.0571	0.7645	
	LL/Cr	0.1461	0.4412	
	ml/Cr	-0.0161	0.9329	
Mean diffusivity (MD)	Cho/Naa	0.1155	0.5435	
	LL/Cr	0.6845	**<.0001***	
	ml/Cr	0.5132	**0.0037***	
Planar tensor (Cp)	Cho/Naa	-0.1556	0.4115	
	LL/Cr	0.3295	0.0754	
	ml/Cr	0.2033	0.2813	
Pure anisotropic diffusion (q)	Cho/Naa	0.1357	0.4745	
	LL/Cr	-0.2034	0.2811	
	ml/Cr	-0.0926	0.6266	
Pure isotropic diffusion (p)	Cho/Naa	0.1155	0.5435	
	LL/Cr	0.6845	**<.0001***	
	ml/Cr	0.5132	**0.0037***	
Radial diffusivity (RD)	Cho/Naa	0.1384	0.4658	
	LL/Cr	0.6933	**<.0001***	
	ml/Cr	0.5082	**0.0041***	
Relative anisotropy (RA)	Cho/Naa	0.1197	0.5286	
	LL/Cr	-0.2294	0.2226	
	ml/Cr	-0.1104	0.5615	
Spherical tensor (Cs)	Cho/Naa	0.1338	0.4809	
	LL/Cr	-0.2883	0.1224	
	ml/Cr	-0.1605	0.3969	
Total magnitude of the diffusion tensor (L)	Cho/Naa	0.1155	0.5435	
	LL/Cr	0.6845	**<.0001***	
	ml/Cr	0.5132	**0.0037***	

Cho/Naa = choline-to-N-acetyl aspartate; LL/Cr = lipids and lactate to creatine; ml/Cr = and myo-inositol/creatine

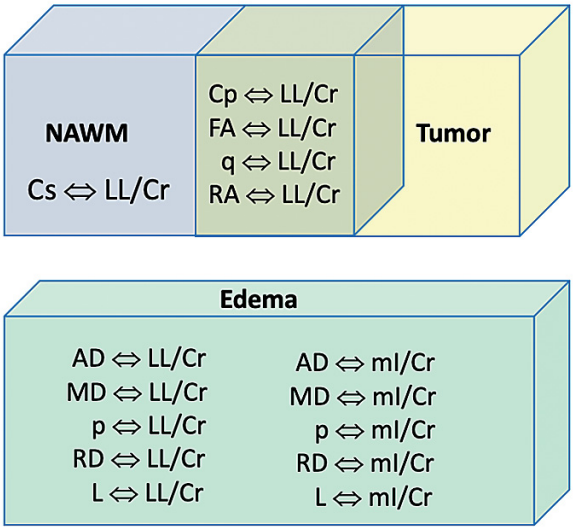

FIGURE 5. Diagram representation of the significant correlations between diffusion tensor imaging (DTI)- magnetic resonance spectroscopy (MRS) biomarkers at the selected regions: normal-appearing white matter (NAWM), enhancing rim and peritumoral edema. Notice that NAWM and the enhancing rim share four pairs of biomarkers correlations; while in peritumoral oedema ten pairs of correlations were exclusive of that region.

structural properties of water molecules and their movements, then the non-significant correlation.

Significant correlations between four DTI metrics and LL/Cr at NAWM and enhancing tumour regions

In our second group of findings, four significant correlations pairs (Cp ⇔ LL/Cr, FA ⇔ LL/Cr, q ⇔ LL/Cr, RA ⇔ LL/Cr) coincidentally appeared in the NAWM and the enhancing tumour regions. They showed some direction of correlation on both region: Three were negative (the more LL/Cr, the less concentration of FA, q and RA); and one positive (LL/Cr and Cp increase or decrease in the same direction).

To understand these relationships, we begin mentioning that creatine, Cr, is a marker of energetic systems and intracellular metabolism; it is considered a stable metabolite for its relatively constant concentration and is used as an internal reference for calculating metabolite ratios.[29] In the combined ratio, LL/Cr, lipid resonances frequently dominate, and lactate (that can be seen in all tumour grades) is mainly present at high levels in glioblastoma.[30]

About the four selected DTI metrics (Cp, FA, q, and RA) that assembled significant bivariate correlations with LL/Cr; FA measures the directionality of water diffusion (shape of the diffusion tensor in each voxel). FA values vary between 0 (isotropic diffusion) and 1 (infinite anisotropy).[31] FA is decreased in glioblastoma.[11] Diffusion is anisotropic in white matter fibre tracts, as axonal membranes and myelin sheaths present barriers to the motion of water molecules, in directions not parallel to their orientation. Reduced FA (water diffusion parallel to axonal tracts) is indicative of axonal degeneration.[32]

We found two articles in the last 15 years mentioning the q biomarker: q is the anisotropic component of the diffusion tensor, with a marked decrease of q in disrupted tracts; q-value in the low-grade tumours is slightly higher than in high-grade tumours, although this is not significantly different.[33] In 2006 Price *et al*. conclude that q may provide a complete picture of the diffusion profile of a brain tumour.[34]

Cp is the planar, geometric representation of the diffusion tensor, and since one decade has been used in the differential diagnosis among abscesses, glioblastomas, and metastases.[11] Mean values of Cp have been quantified at the enhancing rim, peritumoral oedema and NAWM regions.[13]

RA is a ratio of the normalised standard deviations between the anisotropic part of the diffusion coefficient and its isotropic part[35]; it is a function of the variance of the eigenvalues of the diffusion tensor, which is not equal to the variance of the diffusivities along with all directions.[36] It was not surprising to find significant correlations of RA and LL/Cr in NAWM, as it has been reported as one of the best biomarkers to characterise NAWM.[13]

Cs ⇔ LL/Cr, the only significant correlations exclusive of NAWM

Cs and LL/Cr depicted a negative correlation, meaning the increase or decrease in opposite directions. Cs describes the spherical, geometric properties of the diffusion tensor[11]; after RA, Cs is the second DTI metric with the best diagnostic performance to characterise the NAWM.[13] It is not clear for us why Cs ⇔ LL/Cr, was the only significant correlation observed at the NAWM, but not observed in peritumoral oedema and enhancing rim.

Significant bivariate correlations exclusive of the peritumoral region

In our fourth and last group of observations, we found ten significant bivariate correlations only observed in that region (AD ⇔ LL/Cr, MD ⇔ LL/

Cr, p ⇔ LL/Cr, RD ⇔ LL/Cr, L ⇔ LL/Cr, AD ⇔ mI/Cr, MD ⇔ mI/Cr, p ⇔ mI/Cr, RD ⇔ mI/Cr, L ⇔ mI/Cr). All correlations had a positive sign, meaning that any increase in LL/Cr or mI/Cr, will coincide with increases in AD, MD, p, RD and L.

Although scarce, there are independent publications on MRS and DTI metrics that helped us understand better these observations. Firstly, we briefly mention basic concepts of the mI/Cr metabolite ratio, after the five DTI metrics observed for this region (AD, MD, p, RD and L).

mI/Cr includes a range of compounds: phosphatidylinositol, inositol polyphosphate, inositol monophosphate, myo-inositol and, to a smaller extent, glycine; because inositol is elevated within astrocytes, it increased peak is taken as an empirical marker of glial density and proliferation.[37] The exact biological significance of mI/Cr, measurable only at short echo time, had been considered uncertain in gliomas.[21]

MD measures the average motion of water molecules, independent of tissue directionality[31]; it is considered a synonym of the coefficient of diffusion in different space guidelines.[38] Increased MD has been observed in the peritumoral region of high-grade gliomas.[39] The best diagnostic performance by MD in the peritumoral region[13] is explained because it measures the magnitude of molecular motion of water. However, MD does not depend directly on the integrity of myelinated fibre tracts.[35]

p is the isotropic component of the diffusion tensor; p values are significantly higher in the low-grade tumours, possibly reflecting the increased cellularity and restriction of water diffusion in high-grade gliomas; disrupted tracts, however, show a marked increase in p.[33] p showed one of the three best diagnostic performance to characterise peritumoral oedema.[13] AD and RD describes microscopic water movement parallel and perpendicular to the axon tract, respectively; inconsistent changes of RD and AD appeared in axonal injury.[40-42] L represents the total magnitude of the diffusion tensor; it shows an increased mean in peritumoral oedema in glioblastoma.[43]

DTI and MRS features of peritumoral oedema in glioblastoma

Characterisation of peritumoral oedema is one of the most challenging topics in glioblastoma. Discrimination of tumour-infiltrated oedema from vasogenic oedema using DTI metrics has demonstrated conflicting results.[44]

Since last ten years, authors coincide that there is no threshold value at which a clear distinction could be made between tumour infiltration and purely vasogenic oedema; no DTI metric can, by itself, definitively distinguish between these regions.[43] Tumour infiltration may occur in brains that appear normal on T2-weighted images in 40% of cases.[34] Gliosis (measured by mI/Cr), is an astrocytic response to any central nervous system injury, which can occur in perifocal oedema. In the relatively long-standing oedema surrounding glioblastoma, glial fibres assume a more regular arrangement, resulting in more organised water diffusion detected with DTI.[11]

Limitations of the study

Some limitations need to be acknowledged: we did not use the single-voxel technique that it is favourite in clinical practice (widely available, usually good field homogeneity, can be readily performed at short echo times, and is relatively easy to process and interpret). However, its highest single limitation is the lack of ability to determine the spatial heterogeneity of spectral patterns and the fact that only a small number of brain regions can be covered within the time constraints of a routine clinical MR exam.[45] We did not measure metabolite relaxation rates due to scan-time limitations related to a large number of voxels under investigation. We were not able to calculate concentrations of additional metabolites such as glutamine, glutamate, alanine, amino acids, separation of lipids and lactate; they required special software packages ready to fit short-echo and long-echo spectra, such as LCModel[46] and jMRUI[47]; these were not available at our institution when the MRS data for this project were acquired. We would have liked to obtain a higher number of directional motion-probing gradients (MPG) like other studies reporting up to 40- and 81- for the DTI acquisition.[48] It is known that the minimal mathematic requirement for DTI-parameters calculation is 6 independent directional MPG settings.[48] Because the amount of imaging time is limited in most clinical situations, we followed the recommendations of the MRI scanner vendor. Our choice of 25 MPG settings thus involved a trade-off between minimizing directional bias and minimizing scanning time, it also complied with the minimum of 20 unique sampling orientations necessary for a robust estimation of anisotropy.[49]

Our statement that tumour infiltration coexist with vasogenic oedema in a heterogeneous pattern

in the peritumoral region was not confirmed with histopathology. The limited explanations to our findings might support the statement by Pena *et al*. "*it is still not known a priori which tensor measure is the most appropriate to quantify pathological changes in brain tissue*".[23]

Future directions

We acknowledge the unmet need of generalising the MRI studies in glioblastoma acquiring advanced imaging techniques, including perfusion-weighted imaging, MR spectroscopy, and DTI, to assess tumour infiltration.[50] Because the MRS and DTI biomarkers have been measured in other types of tumours[11,16], we believe that the results of this study also apply to those tumours. However, future studies should address if similar correlations are also observed for them. To achieve a deeper understanding of the DTI and MRS interactions; multivariate analysis of DTI metrics and MRS metabolites, controlling the effect of confounders (gender, age, regional location of the tumour, infiltration patterns using MRS and DTI) might unveil unknown interactions of these biomarkers at the ultrastructural level in glioblastoma to support the speculation in our explanations.

We believe MRS and DTI will be incorporated soon in the context of the World Health Organization (WHO) updated the central nervous system (CNS) tumour classification. In the updated 2016 WHO CNS tumour classification version, some tumours were defined by a combination of microscopic morphologic and molecular and genetic factors, whereas others continue to be defined by morphology alone. Although not official, there is a role for DTI and MRS in the current evaluaLaslotion of glioblastoma: IDH1 and IDH2 mutations (which are referred collectively as isocitrate dehydrogenase [IDH] mutation) have become definitional for infiltrating gliomas in adults, with 1p/19q codeletion further characterizing the type.[51] Mutation in IDH1 and IDH2 alters the role of the IDHs in the citric acid cycle and leads to accumulation of the oncometabolite 2-hydroxyglutarate (2HG) within tumour cells. Although IDH mutants themselves do not present a clear radiologic signature, 2HG can be detected at MR spectroscopy.[52] The 1p/19q codeletion is associated with the apparent diffusion coefficient value[53], which is equivalent to the MD[24], a DTI metric that had significant Rs in our study. Routine use of advanced MRI in glioblastoma has been incorporated into glioma imaging protocols at some institutions.[51]

Conclusions

A comprehensive understanding of appropriate DTI and MRS biomarkers for each tumour region in glioblastoma would obtain complementary metabolic and ultrastructural information necessary to preoperatively identify sites of significant tumour infiltration that appear normal on conventional MRI and in the follow-up of glioblastoma patients. DTI, in combination with MRS, are additional tools of the "biologic targeting" for radiation therapy. DTI and MRS biomarkers answer different questions; peritumoral oedema represents the biggest challenge with at least ten significant correlations between DTI and MRS that need additional studies. The fact that DTI and MRS measures are not specific of one histologic type of tumour broadens their application to a wider variety of intracranial pathologies. Correlation maps between DTI and MRS might help researchers supplement the diagnosis and treatment planning of brain tumours, decreasing the underlying empiricism in this area.

Acknowledgement

Eduardo Flores-Alvarez was supported by Consejo Nacional de Ciencia y Tecnologia (CONACyT), Mexico, fellowship award. This work was submitted in partial fulfilment of the requirements for the DSc degree of Eduardo Flores-Alvarez at the Programa de Doctorado en Ciencias Medicas, Facultad de Medicina, Universidad Nacional Autónoma de Mexico.

References

1. Tugcu B, Postalci LS, Gunaldi O, Tanriverdi O, Akdemir H. Efficacy of clinical prognostic factors on survival in patients with glioblastoma. *Turk Neurosurg* 2010; **20:** 117-25. doi: 10.5137/1019-5149.JTN.2461-09.4

2. Seidel C, Dörner N, Osswald M, Wick A, Platten M, Bendszus M, et al. Does age matter? - A MRI study on peritumoral edema in newly diagnosed primary glioblastoma. *BMC cancer* 2011; **11:** 127. doi: 10.1186/1471-2407-11-127

3. Perez-Beteta J, Molina-García D, Martínez-González A, Henares-Molina A, Amo-Salas M, Luque B, et al. Morphological MRI-based features provide pretreatment survival prediction in glioblastoma. *Eur Radiol* 2019; **29:** 1968-77. doi: 10.1007/s00330-018-5758-7

4. Blomstergren A, Rydelius A, Abul-Kasim K, Lätt J, Sundgren PC, Bengzon J. Evaluation of reproducibility in MRI quantitative volumetric assessment and its role in the prediction of overall survival and progression-free survival in glioblastoma. *Acta Radiol* 2019; **60:** 516-25. doi: 10.1177/0284185118786060

5. Abbasi AW, Westerlaan HE, Holtman GA, Aden KM, van Laar PJ, van der Hoorn A. Incidence of tumour progression and pseudoprogression in high-grade gliomas: a systematic review and meta-analysis. *Clin Neuroradiol* 2018; **28:** 401-11. doi: 10.1007/s00062-017-0584-x

6. Durand-Munoz C, Flores-Alvarez E, Moreno-Jimenez S, Roldan-Valadez E. Pre-operative apparent diffusion coefficient values and tumour region volumes as prognostic biomarkers in glioblastoma: correlation and progression-free survival analyses. *Insights Imaging* 2019; **10:** 36. doi: 10.1186/s13244-019-0724-8

7. Zikou A, Sioka C, Alexiou GA, Fotopoulos A, Voulgaris S, Argyropoulou MI. Radiation necrosis, pseudoprogression, pseudoresponse, and tumor recurrence: imaging challenges for the evaluation of treated gliomas. *Contrast Media Mol Imaging* 2018; **2018:** 6828396. doi: 10.1155/2018/6828396

8. Cordova JS, Shu HK, Liang Z, Gurbani SS, Cooper LA, Holder CA, et al. Whole-brain spectroscopic MRI biomarkers identify infiltrating margins in glioblastoma patients. *Neuro Oncol* 2016; **18:** 1180-9. doi: 10.1093/neuonc/now036

9. van Dijken BRJ, van Laar PJ, Holtman GA, van der Hoorn A. Diagnostic accuracy of magnetic resonance imaging techniques for treatment response evaluation in patients with high-grade glioma, a systematic review and meta-analysis. *Eur Radiol* 2017; **27:** 4129-44. doi: 10.1007/s00330-017-4789-9

10. Roldan-Valadez E, Rios C, Motola-Kuba D, Matus-Santos J, Villa AR, Moreno-Jimenez S. Choline-to-N-acetyl aspartate and lipids-lactate-to-creatine ratios together with age assemble a significant Cox's proportional-hazards regression model for prediction of survival in high-grade gliomas. *Br J Radiol* 2016; **89:** 20150502. doi: 10.1259/bjr.20150502

11. Toh CH, Wei KC, Ng SH, Wan YL, Lin CP, Castillo M. Differentiation of brain abscesses from necrotic glioblastomas and cystic metastatic brain tumors with diffusion tensor imaging. *AJNR Am J Neuroradiol* 2011; **32:** 1646-51. doi: 10.3174/ajnr.A2581

12. Roldan-Valadez E, Rios C, Cortez-Conradis D, Favila R, Moreno-Jimenez S. Global diffusion tensor imaging derived metrics differentiate glioblastoma multiforme vs. normal brains by using discriminant analysis: introduction of a novel whole-brain approach. *Radiol Oncol* 2014; **48:** 127-36. doi: 10.2478/raon-2014-0004

13. Cortez-Conradis D, Favila R, Isaac-Olive K, Martinez-Lopez M, Rios C, Roldan-Valadez E. Diagnostic performance of regional DTI-derived tensor metrics in glioblastoma multiforme: simultaneous evaluation of p, q, L, Cl, Cp, Cs, RA, RD, AD, mean diffusivity and fractional anisotropy. *Eur Radiol* 2013; **23:** 1112-21. doi: 10.1007/s00330-012-2688-7

14. Rees JH, Smirniotopoulos JG, Jones RV, Wong K. Glioblastoma multiforme: radiologic-pathologic correlation. *Radiographics* 1996; **16:** 1413-38; quiz 1462-3. doi: 10.1148/radiographics.16.6.8946545

15. Tang CY, Friedman J, Shungu D, Chang L, Ernst T, Stewart D, et al. Correlations between diffusion tensor imaging (DTI) and magnetic resonance spectroscopy (1H MRS) in schizophrenic patients and normal controls. *BMC Psychiatry* 2007; **7:** 25. doi: 10.1186/1471-244X-7-25

16. Brandao LA, Domingues RC. Brain metabolites and their significance in spectral analysis. In: Brandao LA, Domingues RC, editors. *MR spectroscopy of the brain.* Philadelphia, PA: Lippincott Williams & Wilkins; 2004. p. 11-2.

17. Browner WS, Newman TB, Hulley SB. Total sample size required when using the correlation coefficient (r). Appendix 6c. In: Hulley SB, Cummings SR, Browner WS, Grady DG, Newman TB. *Designing clinical research.* Philadelphia, PA: Lippincott, Williams & Wilkins; 2013. p. 79.

18. Chan YH. Biostatistics 104: correlational analysis. *Singapore Med J* 2003; **44:** 614-9. PMID: 14770254

19. Barton B, Peat J. Correlation coefficients. Chapter 7. In: Barton B, Peat J, editors. *Medical statistics. A guide to SPSS, data analysis and critical appraisal.* West Sussex, UK: John Wiley & Sons Ltd; 2014. p. 197-204.

20. Pallant J. Testing the statistical significance of the difference between correlation coefficients. In: Pallant J, editor. *SPSS survival manual.* Crows Nest, NSW, Australia: Allen & Unwin; 2011. p. 139-41.

21. Waldman AD, Jackson A, Price SJ, Clark CA, Booth TC, Auer DP, et al. Quantitative imaging biomarkers in neuro-oncology. *Nat Rev Clin Oncol* 2009; **6:** 445-54. doi: 10.1038/nrclinonc.2009.92

22. Sadeghi N, Camby I, Goldman S, Gabius HJ, Balériaux D, Salmon I, et al. Effect of hydrophilic components of the extracellular matrix on quantifiable diffusion-weighted imaging of human gliomas: preliminary results of correlating apparent diffusion coefficient values and hyaluronan expression level. *AJR Am J Roentgenol* 2003; **181:** 235-41. doi: 10.2214/ajr.181.1.1810235

23. Peña A, Green HA, Carpenter TA, Price SJ, Pickard JD, Gillard JH. Enhanced visualization and quantification of magnetic resonance diffusion tensor imaging using the p:q tensor decomposition. *Br J Radiol* 2006; **79:** 101-9. doi: 10.1259/bjr/24908512.

24. Cortez-Conradis D, Rios C, Moreno-Jimenez S, Roldan-Valadez E. Partial correlation analyses of global diffusion tensor imaging-derived metrics in glioblastoma multiforme: Pilot study. *World J Radiol* 2015; **7:** 405-14. doi: 10.4329/wjr.v7.i11.405

25. Bitsch A, Bruhn H, Vougioukas V, Stringaris A, Lassmann H, Frahm J, et al. Inflammatory CNS demyelination: histopathologic correlation with in vivo quantitative proton MR spectroscopy. *AJNR Am J Neuroradiol* 1999; **20:** 1619-27. PMID: 10543631

26. Barker PB, Soher BJ, Blackband SJ, Chatham JC, Mathews VP, Bryan RN. Quantitation of proton NMR spectra of the human brain using tissue water as an internal concentration reference. *NMR in biomedicine* 1993; **6:** 89-94. doi: 10.1002/nbm.1940060114

27. Gasparovic C, Arfai N, Smid N, Feeney DM. Decrease and recovery of N-acetylaspartate/creatine in rat brain remote from focal injury. *J Neurotrauma* 2001; **18:** 241-6. doi: 10.1089/08977150151070856

28. Law M, Yang S, Wang H, Babb JS, Johnson G, Cha S, et al. Glioma grading: sensitivity, specificity, and predictive values of perfusion MR imaging and proton MR spectroscopic imaging compared with conventional MR imaging. *AJNR Am J Neuroradiol* 2003; **24:** 1989-98. doi:

29. Bertholdo D, Watcharakorn A, Castillo M. Proton magnetic resonance spectroscopy. Introduction and overview. In: Brandao LA, editor. *MR spectroscopy of the brain.* Philadelphia, PA: Elsevier Inc.; 2013. p. 359-80.

30. Stadlbauer A, Gruber S, Nimsky C, Fahlbusch R, Hammen T, Buslei R, et al. Preoperative grading of gliomas by using metabolite quantification with high-spatial-resolution proton MR spectroscopic imaging. *Radiology* 2006; **238:** 958-69. doi: 10.1148/radiol.2382041896

31. Pierpaoli C, Basser PJ. Toward a quantitative assessment of diffusion anisotropy. *Magn Reson Med* 1996; **36:** 893-906. doi: 10.1002/mrm.1910360612

32. Neil J, Miller J, Mukherjee P, Hüppi PS. Diffusion tensor imaging of normal and injured developing human brain - a technical review. *NMR in biomedicine* 2002; **15:** 543-52. doi: 10.1002/nbm.784

33. Price SJ, Peña A, Burnet NG, Jena R, Green HA, Carpenter TA, et al. Tissue signature characterisation of diffusion tensor abnormalities in cerebral gliomas. *Eur Radiol* 2004; **14:** 1909-17. doi: 10.1007/s00330-004-2381-6

34. Price SJ, Jena R, Burnet NG, Hutchinson PJ, Dean AF, Peña A, et al. Improved delineation of glioma margins and regions of infiltration with the use of diffusion tensor imaging: an image-guided biopsy study. *AJNR Am J Neuroradiol* 2006; **27:** 1969-74.

35. Le Bihan D, Mangin JF, Poupon C, Clark CA, Pappata S, Molko N, et al. Diffusion tensor imaging: concepts and applications. *J Magn Reson Imaging* 2001; **13:** 534-46. doi: 10.1002/jmri.1076

36. Ozarslan E, Vemuri BC, Mareci TH. Generalized scalar measures for diffusion MRI using trace, variance, and entropy. *Magn Reson Med* 2005; **53:** 866-76. doi: 10.1002/mrm.20411

37. Minati L, Aquino D, Bruzzone MG, Erbetta A. Quantitation of normal metabolite concentrations in six brain regions by in-vivoH-MR spectroscopy. *Med Phys* 2010; **35:** 154-63. doi: 10.4103/0971-6203.62128

38. Mori S, Barker PB. Diffusion magnetic resonance imaging: its principle and applications. *Anat Rec* 1999; **257:** 102-9. doi: 10.1002/(SICI)1097-0185(19990615)257:3<102::AID-AR7>3.0.CO;2-6

39. Lu S, Ahn D, Johnson G, Cha S. Peritumoral diffusion tensor imaging of high-grade gliomas and metastatic brain tumors. *AJNR Am J Neuroradiol* 2003; **24:** 937-41.

40. Budde MD, Xie M, Cross AH, Song SK. Axial diffusivity is the primary correlate of axonal injury in the experimental autoimmune encephalomyelitis spinal cord: a quantitative pixelwise analysis. *J Neurosci* 2009; **29:** 2805-13. doi: 10.1523/JNEUROSCI.4605-08.2009

41. Song SK, Sun SW, Ramsbottom MJ, Chang C, Russell J, Cross AH. Dysmyelination revealed through MRI as increased radial (but unchanged axial) diffusion of water. *Neuroimage* 2002; **17:** 1429-36. doi: 10.1006/nimg.2002.1267

42. Zhang X, Sun P, Wang J, Wang Q, Song SK. Diffusion tensor imaging detects retinal ganglion cell axon damage in the mouse model of optic nerve crush. *Invest Ophthalmol Vis Sci* 2011; **52:** 7001-6. doi: 10.1167/iovs.11-7619

43. Wang W, Steward CE, Desmond PM. Diffusion tensor imaging in glioblastoma multiforme and brain metastases: the role of p, q, L, and fractional anisotropy. *AJNR Am J Neuroradiol* 2009; **30:** 203-8. doi: ajnr.A1303 [pii]10.3174/ajnr.A1303

44. Lu S, Ahn D, Johnson G, Law M, Zagzag D, Grossman RI. Diffusion-tensor MR imaging of intracranial neoplasia and associated peritumoral edema: introduction of the tumor infiltration index. *Radiology* 2004; **232:** 221-8. doi: 10.1148/radiol.2321030653

45. Barker PB, Bizzi A. Stefano ND, Gullapalli RP, Lin DDM. *Clinical MR spectroscopy. Techniques and Applications.* Cambridge, UK: Cambridge University Press; 2010.

46. Provencher SW. Automatic quantitation of localized in vivo 1H spectra with LCModel. *NMR Biomed* 2001; **14:** 260-4. doi: 10.1002/nbm.698

47. Naressi A, Couturier C, Castang I, de Beer R, Graveron-Demilly D. Java-based graphical user interface for MRUI, a software package for quantitation of in vivo/medical magnetic resonance spectroscopy signals. *Comput Biol Med* 2001; **31:** 269-86. doi: 10.1016/s0010-4825(01)00006-3

48. Yamamoto A, Miki Y, Urayama S, Fushimi Y, Okada T, Hanakawa T, et al. Diffusion tensor fiber tractography of the optic radiation: analysis with 6-, 12-, 40-, and 81-directional motion-probing gradients, a preliminary study. *AJNR Am J Neuroradiol* 2007; **28:** 92-6.

49. Jones DK. The effect of gradient sampling schemes on measures derived from diffusion tensor MRI: a Monte Carlo study. *Magn Reson Med* 2004; **51:** 807-15. doi: 10.1002/mrm.20033

50. Bette S, Huber T, Gempt J, Boeckh-Behrens T, Wiestler B, Kehl V, et al. Local fractional anisotropy is reduced in areas with tumor recurrence in glioblastoma. *Radiology* 2017; **283:** 499-507. doi: 10.1148/radiol.2016152832

51. Johnson DR, Guerin JB, Giannini C, Morris JM, Eckel LJ, Kaufmann TJ. 2016 updates to the WHO brain tumor classification system: What the radiologist needs to know. *Radiographics* 2017; **37:** 2164-80. doi: 10.1148/rg.2017170037

52. Pope WB, Prins RM, Albert Thomas M, Nagarajan R, Yen KE, Bittinger MA, et al. Non-invasive detection of 2-hydroxyglutarate and other metabolites in IDH1 mutant glioma patients using magnetic resonance spectroscopy. *J Neurooncol* 2012; **107:** 197-205. doi: 10.1007/s11060-011-0737-8

53. Johnson DR, Diehn FE, Giannini C, Jenkins RB, Jenkins SM, Parney IF, et al. Genetically defined oligodendroglioma is characterized by indistinct tumor borders at MRI. *AJNR Am J Neuroradiol* 2017; **38:** 678-84. doi: 10.3174/ajnr.A5070